Prolonged rock exhumation at the rims of kilometer-scale lunar craters

Cole A. Nypaver[1], Bradley J. Thomson[1], Caleb I. Fassett[2], Edgard G. Rivera-Valentín[3], Gerald W. Patterson[4]

[1]Department of Earth and Planetary Sciences, University of Tennessee Knoxville, TN, 37966. [2]NASA Marshall Space Flight Center, Huntsville, AL 35805. [3]Lunar and Planetary Institute, Universities Space Research Association, Houston, TX 77058. [4]The Johns Hopkins University Applied Physics Laboratory, 11100 Johns Hopkins Rd., Laurel, MD 20723

Corresponding author: Cole Nypaver (cnypaver@vols.utk.edu)

Key Points:

- Rocks at kilometer-scale impact crater rims are continually being uncovered due to the downslope movement of the overlying regolith.
- Topographic rims associated with 0.5–2.0 km diameter lunar impact craters retain surface rock populations for >3.0 Ga.
- Lunar sample collection at impact crater rims may yield material that is unlikely to have undergone transport from other areas of the Moon.

Abstract

Fresh impact ejecta deposits on the lunar surface can be characterized as heterogeneous mixtures of boulders, cobbles, and fine-grained regolith that are deposited on the lunar surface during the impact crater formation process. Over time, the boulders associated with ejecta deposits break down into fine-grained regolith due to a combination of bombardment and thermal fatigue. Several qualitative observations of old (>2.0 Ga) kilometer-scale lunar impact ejecta deposits made here in high-resolution images reveal tens of large (>1 m) boulders associated with kilometer-scale crater rims and near-proximal ejecta deposits on the lunar maria. These observations went undescribed in prior measurements of lunar boulder breakdown which suggested that lunar boulders should be destroyed in <300 Myr due to micrometeoroid impacts and other processes (e.g., Basilevsky et al., 2015). Here, we use a combination of radar and thermal-infrared data from the Lunar Reconnaissance Orbiter spacecraft to show that kilometer-scale impact crater rims exhibit elevated rock abundances for the lifetime of the lunar maria. We interpret these results as indicating that boulders are continually being uncovered at crater rims due to downslope movement of the overlying regolith. Moreover, rocks found at crater rims that have been exhumed from depth in geologically recent times are locally derived and unlikely to have come from other areas of the Moon. Future collection of lunar samples at crater rims will serve to mitigate the potential for sample contamination from distal sources, helping to ensure accurate geologic interpretations from the collected samples.

Plain Language Summary

Any asteroid or comet that strikes the surface of the Moon will produce and deposit a mixture of large rocks and fine-grained soil, known as ejecta, on the lunar surface. The result of the numerous impacts of all scales that have occurred on the Moon is that the entire surface is covered by a regolith made up of dust, sand, and pulverized rocks. Exposed rocks in the regolith on the lunar surface are broken down over time and reduced in size, likely due to impact from other meteoroids and thermal expansion and contraction. Prior studies have observed that rock breakdown takes no longer than ~300 million years for >2m boulders. Here, we observe boulders present at the rims of two-to-three billion year old impact craters. Reconciling these observations is possible if rocks at the rims of lunar impact craters are being continually uncovered due to the downslope movement of overlying lunar regolith. Moreover, because they are uncovered from the subsurface, rocks at crater rims are less likely to have undergone transport from another part of the Moon, which makes them an attractive potential source for future lunar samples.

1 Introduction

The On the surface of Earth's Moon, impact craters exhibit distinct morphologies that often correlate to crater diameter (e.g., Melosh, 1989; Stöffler et al., 2006). The impact crater formation process has been extensively modelled and simulated in the laboratory setting (e.g., Schmidt and Housen, 1987), but the post-formation breakdown processes undergone by impact craters on the lunar surface remains an area of ongoing research (e.g., Soderblom, 1970; Craddock and Howard, 2000; Fassett and Thomson, 2014; Minton et al., 2019). Recent remote sensing data provided by the Lunar Reconnaissance Orbiter (LRO) have helped to improve our understanding of the geomorphic effects of lunar surface exposure on impact crater morphology and crater ejecta deposit characteristics (e.g., Neish et al., 2013; Ghent et al., 2014; 2016; Fassett et al., 2018; Wang et al., 2020). However, many questions remain regarding the rate that impact

ejecta deposits are modified, the mechanisms responsible for crater degradation, and the reliability of remote sensing data for assessing these geologic processes.

Recent work using S-band (12.6 cm, 2380 MHz) radar data from the LRO Miniature Radio-Frequency (Mini-RF) instrument revealed that while surface and subsurface rock populations associated with lunar impact ejecta are diminished with time due to space weathering processes, the rock content of impact crater interiors increases for the first ~0.5 Gyr of a crater's lifetime (Fassett et al., 2018). A separate study used thermal infrared measurements from the LRO Diviner instrument to show that ejecta deposits associated with large lunar impact craters break down at a measurable rate, and that rate could be used to infer an approximate age for large impact craters on the lunar surface (Ghent et al., 2014; 2016). The rate of ejecta breakdown established by that work was more recently utilized to infer an increase in the inner solar system cratering rate at approximately ~290 Ma (Mazrouei et al., 2019). Lastly, several studies have utilized high-resolution images from the Lunar Reconnaissance Orbiter Camera (LROC) to manually count the number of boulders present in lunar ejecta deposits associated with craters of varying ages (e.g., Basilevsky et al., 2013; 2015; 2018; Li et al., 2018; Watkins et al., 2019). Those data were used to infer that boulders ≥2m on the lunar surface are destroyed in less than 300 Myr, likely due to meteoroid impacts and thermal fatigue of exposed rocks at the lunar surface (e.g., Hörz et al., 1975; Molaro et al., 2017). These studies indicate that the post formation fate of impact craters and impact ejecta is far from simple and breakdown processes are not well understood. The variations in boulder breakdown timing between optical and remote-sensing based studies are likely due to some combination of poorly constrained crater age estimates, variations in study-crater diameters, and the expectation that ejecta deposits break down homogenously. Lunar impact crater ages are notoriously difficult to establish (e.g., Robbins et al., 2014). Past studies have established crater ages by utilizing interior crater counting methods and qualitative morphology comparisons with craters that possess radiometric age dates from Apollo samples. In separate analyses of boulder breakdown, which utilized the rock sensitivities of thermal and radar data, the studied craters exhibited larger (~18–97 km) diameters (Ghent et al., 2014). Craters of that size exhibit much larger boulders and more extensive ejecta deposits (e.g., Bart and Melosh, 2010). Those larger craters also break down much differently through time when compared to their km-scale counterparts in optical-based boulder breakdown studies (e.g., Fassett et al., 2019a; Minton et al., 2019).

Many of these prior studies examined the breakdown of ejecta constituents as a whole without accounting for intra-ejecta variations in rock population breakdown rate. In a visual assessment of old (>2.0 Gyr) kilometer-scale craters on the lunar maria, we observed tens of large (>1.0 m) boulders associated with the ejecta on and just outside of the impact crater rims with a lack of boulders beyond that narrow annular zone (Fig. 1). Based on these initial observations, we develop a working hypothesis that a population of boulders can be found at crater rims for an extended period of time. To test this hypothesis, we focus on the modification rates for crater rims and impact ejecta deposits associated with 6,221 small (<2 km) simple impact craters on the lunar maria using a combination of radar data from the LRO Mini-RF instrument and Rock Abundance data derived from LRO Diviner thermal radiometer measurements (Fig. 2). Our results indicate that the survival time of rock populations differ drastically for impact crater rims and ejecta deposits. We infer this finding to indicate that rocks at km-scale impact crater rims are continuously being exhumed (i.e., uncovered from beneath an overlying mobile regolith) for >3.0 Gyr. Lunar impact crater rims are, therefore, ideal locations for the collection of future lunar samples whose origin can be determined. Given that crater

production rates are inherently tied to radiometric age dates of collected lunar samples, further sampling of the lunar surface will be crucial for constraining surface age models of the Moon and other inner solar system planets.

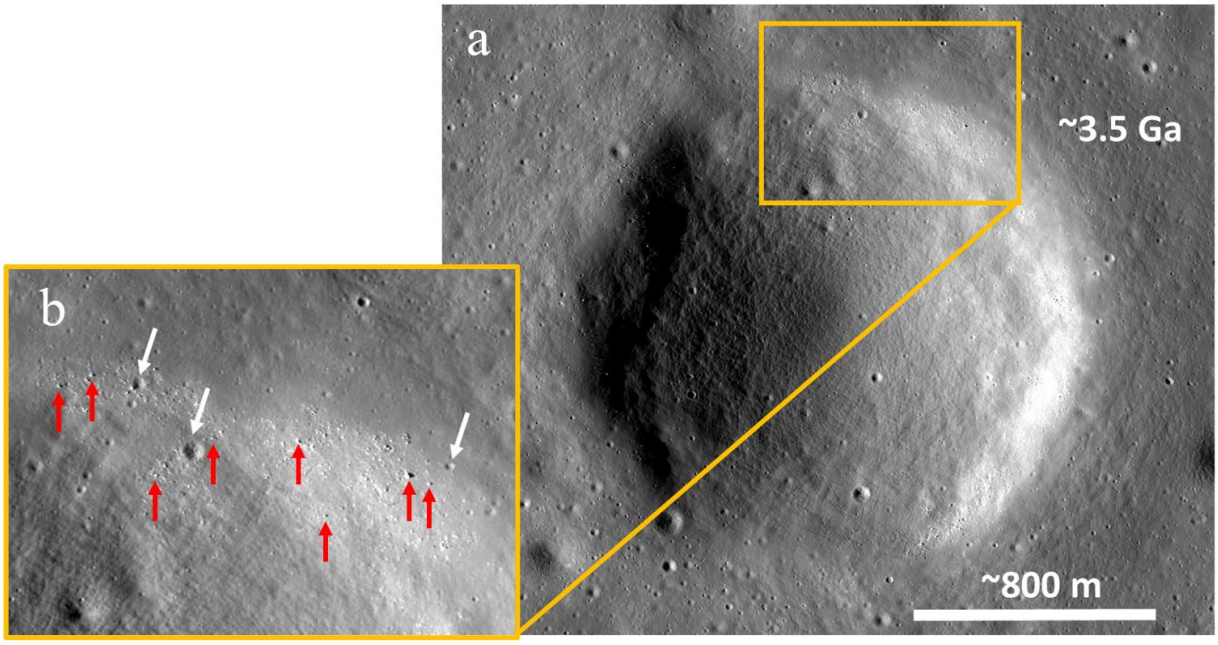

Figure 1. (a) LROC NAC image of a simple impact crater with a diameter of ~2.0 km on Mare Nubium (20.206° N, 9.031° E) with a modelled age of ~3.7 Ga (κt: 26203, Fassett and Thomson, 2014) and a (b) enhanced image of the NE portion of the crater rim with red arrows indicating boulders present in this region and white arrows indicating small impact craters amongst the boulders.

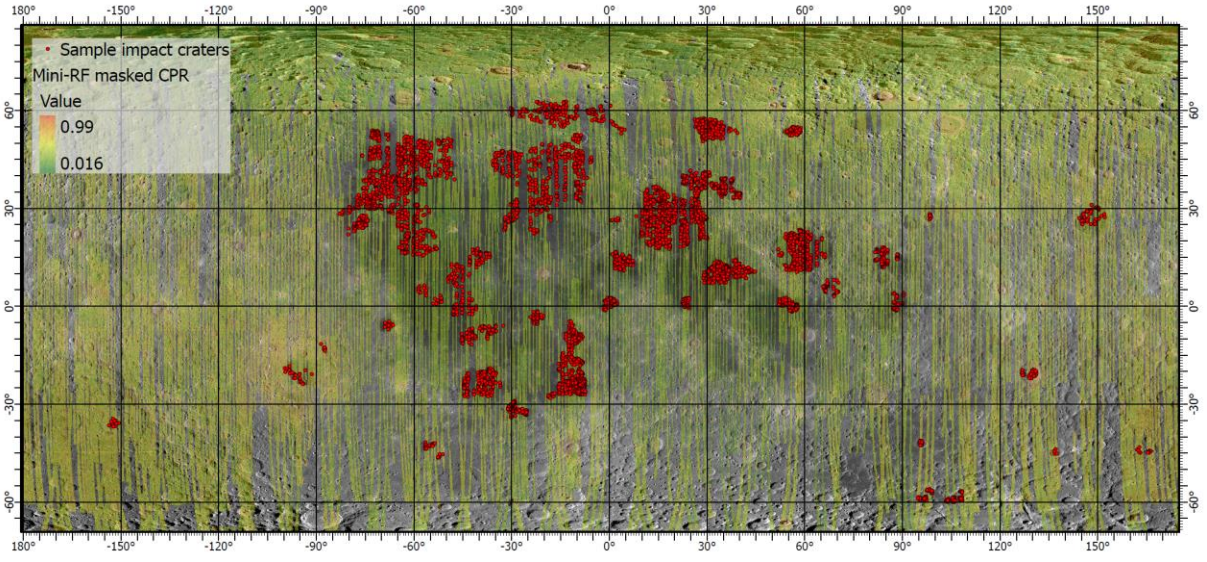

Figure 2. Locations of individual sample craters from the Fassett and Thomson, 2014 crater database (red points) superposed onto Mini-RF CPR and LROC WAC global mosaics.

2 Background

Macroscopic space weathering is the primary means by which rocks on the lunar surface break down over time due to a lack of atmospheric winds and liquid water (e.g., Hörz et al., 1975; Hörz and Cintala, 1985). The processes responsible for lunar rock breakdown are meteoroid bombardment and thermal cycling. Micrometeoroid bombardment is defined as the continual sandblasting of lunar rocks by small (~10^{-15}–10^{-3} g) meteoroids which reduce that boulder into small fragments over time (e.g., Ross, 1968; Soderblom, 1970). Larger impactors also contribute to the boulder breakdown process at the lunar surface. While larger, cm-scale impactors occur less frequently than micrometeoroid impacts, the likelihood of a larger impactor imparting a critical rupture energy on a lunar boulder is much higher. Thermal fatigue and shock are the responses of lunar boulders to the intense temperature fluctuations of the lunar day-night cycle (e.g., Molaro and Byrne, 2012; Molaro et al., 2017). Thermal fatigue results in microcrack propagation within the boulder while thermal shock is the catastrophic rupture of a boulder due to overwhelming microcrack propagation. Although described separately here, all of these breakdown processes act together as a continuum of rock fragmentation. The relative contribution of these physical breakdown mechanisms to the breakdown of lunar rocks remains a topic of ongoing research. Prior work has modelled the time required for these processes to reduce boulders on the lunar surface to fine-grained regolith (e.g., Basilevsky et al 2013; 2015; Watkins et al., 2019). Those prior studies use high resolution LROC images to manually count the boulders present on various impact ejecta blankets and compare those distributions with the modelled age of the impact crater to establish boulder lifetimes. Results generally agree that even the largest boulders on the lunar surface should be completely broken down in no longer than ~300 Myr (e.g., Basilevsky et al., 2013; Watkins et al., 2019).

While boulders are present in other locations on the lunar surface such as rilles, wrinkle ridges, and domes, impact craters and associated ejecta blankets have been the main study sites for examining boulder populations and lifetimes on the lunar surface. Past analyses of lunar boulder breakdown have focused on ejecta deposits associated with km-scale craters largely due to the consistent presence of meter-scale boulders within them. Because the Moon lacks a meaningful atmosphere, boulders are emplaced ballistically during the impact crater formation process. The majority of boulders produced during crater formation are emplaced within ~2–3 crater radii of the parent crater in the proximal ejecta deposit, but some can be distributed several tens to hundreds of kilometers as part of the distal ejecta (e.g., Osinski et al., 2011). Furthermore, these boulders are emplaced in a pattern of gradational size with the largest boulders near the rim of the parent crater and boulder diameter subsequently decreasing in size with distance from the rim (e.g., Bart and Melosh, 2010).

The data used to assess rock populations in this work are derived products from the Miniature Radio Frequency (Mini-RF) and Diviner instruments onboard the Lunar Reconnaissance Orbiter (LRO). The Mini-RF instrument is a hybrid, dual-polarization Synthetic Aperture Radar (SAR) that transmits a left-circular polarized signal and receives the horizonal and vertical components of that signal. Reflection of the incident, left-polarized signal from a single scattering event at the lunar surface results in a returned signal in the opposite circular (OC) polarization as transmitted. This single scattering event is referred to as specular scattering and commonly occurs in association with smooth, featureless surfaces. In contrast to specular scattering, multiple scattering events at the lunar surface commonly result in a signal polarization

change to the same circular (SC) polarization as transmitted. The multiple scattering behavior is referred to as diffuse scattering, which is commonly associated with areas of the lunar surface and subsurface where wavelength-scale boulders are abundant. The SC component of the radar signal is enhanced by reflectors that are within an order of magnitude of the radar wavelength in size on the lunar surface and down to a depth of some 10× the radar wavelength (Campbell & Ulrichs, 1969). The OC component is enhanced by single reflections from relatively flat, undisturbed surfaces (i.e., the lunar soil-atmosphere horizon). A comparison of these components will reveal the relative contributions of the various scatter-causing mechanisms to the returned radar signal. Several recent studies have utilized SC and OC data from the Mini-RF instrument, specifically, to assess roughness and potential ice associated with lunar impact craters (Thompson et al., 2011; Virkki and Bhiravarasu, 2019). These data are important for the work here in that an enhanced SC component associated with the radar return at the rims of older craters in our dataset may support our hypothesis that boulders are present at these locations for extended periods of time.

An additional radar product that we utilize in this work is circular polarization ratio (CPR) data from the Mini-RF instrument. These CPR data is the ratio of the SC and OC radar albedo. Prior studies have revealed that CPR data serve as a useful metric for assessing surface and subsurface rock populations on the Moon (e.g., Fa et al., 2011; Campbell, 2012). Given the direct and inverse dependencies on the SC and OC polarization components, respectively, a densely bouldered surface will increase CPR while a relatively smooth surface will exhibit a lower CPR. The rough surface with an abundance of surface and subsurface boulders on the scale of the S-band wavelength will exhibit a characteristically higher CPR because of the likelihood of multiple interactions at the S-band radar wavelength-scale.

The thermal infrared dataset that we use to measure rock and boulder populations in lunar ejecta deposits is rock abundance (RA) data (Bandfield et al., 2011; 2015). A derivation of thermal infrared instruments from the Diviner instrument onboard LRO, RA represents the areal fraction of the lunar surface that is covered in rocks ~1 m in diameter. The RA model assumes input parameters of density, specific heat capacity, and thermal conductivity for a vesicular basalt (Horai and Simmons, 1972) to define a rock thermal inertia of 1570 J m^{-2} K^{-1} $s^{-1/2}$ at 200 K for the lunar surface. This thermal inertia, an emissivity of 0.95, and an albedo of 0.15 were then used to construct a rock temperature lookup table and model the radiance of the lunar surface. Rock temperatures were binned by latitude and local lunar time and the radiance was compared for each bin. Model rock abundance was then obtained by minimizing the root mean squared error between the measured and model radiance values. Rock abundance ranges from 0.05–0.1 (5–10%) on the lunar maria but can theoretically reach values of 1 (100%) where surface rocks comprise the entire lunar surface (Bandfield et al., 2011, 2015). Both the Mini-RF radar and Diviner RA data are publicly available in global mosaic form from the University of Washington, St. Louis Planetary Data System Geosciences node (https://pds-geosciences.wustl.edu/missions/lro/).

In order to compare the age of craters to their boulder populations, ages for the associated impact craters must first be established. The crater ages used in this work were modelled from topographic degradation state in Fassett and Thomson (2014; hereafter referred to as FT2014). In that study, the authors extracted topographic profiles from ~13,000 km-scale impact craters on the lunar maria in the size range of ~0.8-5.0 km from topography data from Kaguya's Terrain Camera (Haruyama et al., 2012). They fit these topographic profiles to a diffusion model to assign topographic degradation states for each crater in their dataset, κt, where κ represents the

integrated diffusivity experienced and *t* represents the time exposed on the Moon. The degradation states were then calibrated to absolute ages by calculating the local crater density of the surface they were exposed on in moving neighborhoods of 50 km radius. The result of this algorithm is a sample set of ~13,000 simple impact craters on the lunar maria with unique degradation states and modelled age values. This degradation model is based on the premise that the features of a fresh impact crater become topographically muted over time due to the downslope motion of the overlying regolith. Until recently, the downslope motion of the regolith covering the crater rims and interior walls has been attributed to ejecta splashing from subsequent primary impactors. The FT2014 crater dataset was recently updated to account for anomalous diffusion (Fassett et al., 2018a). Anomalous diffusion is defined as the combination of small, primary impacts and distal, secondary impacts into a pre-existing, larger impact structure with a net downslope ejecta distribution that subsequently flattens topographic slopes over time (Speyerer et al., 2016; Fassett et al., 2018a; Minton et al., 2019). This update corrected the individual κt values to account for the size-dependence of topographic diffusion by normalizing the diffusion model to a 1-km crater diameter. This is an improvement on the prior description of the crater degradation process (e.g., Xie et al., 2017) and is necessary to reconcile crater degradation with the observed equilibrium size-frequency distributions observed on the lunar surface (Minton et al., 2019). Seismic shaking may also contribute to the process of topographic degradation. However, prior work has demonstrated that seismic shaking, when compared to the process of ballistic sedimentation-driven diffusion, is likely a secondary process in topographic degradation on the Moon (Fassett et al., 2011).

3 Methods

The sample set of craters used for this study consists of those craters from the FT2014 and Fassett et al., 2018 database convolved with Mini-RF data coverage (6,221 craters) and Diviner RA data coverage (6,240 craters). This slightly larger sample set of craters measured in the RA data is due to better RA data coverage over the lunar mare. Using ArcMap 10.6, the center points of these craters were overlain as a single shapefile onto the Mini-RF CPR, SC and OC radar albedo, and Diviner Rock Abundance global mosaics (Fig. 3). Because the Mini-RF and Diviner RA mosaics exhibit imperfect selenodetic control with the LROC WAC basemap, offsets no greater than ~1.0 km existed between the WAC, RA, and radar mosaics. To correct for these offsets and ensure consistent annular zone boundaries, all center points were manually re-referenced to the geographic centers of the respective crater in each dataset. The ArcMap Zonal Statistics tool was then used to extract average CPR, SC, OC, and RA values associated with the crater rims (1.0-1.5 crater radii) and proximal ejecta deposits (1.5-4.0 crater radii) of each crater.

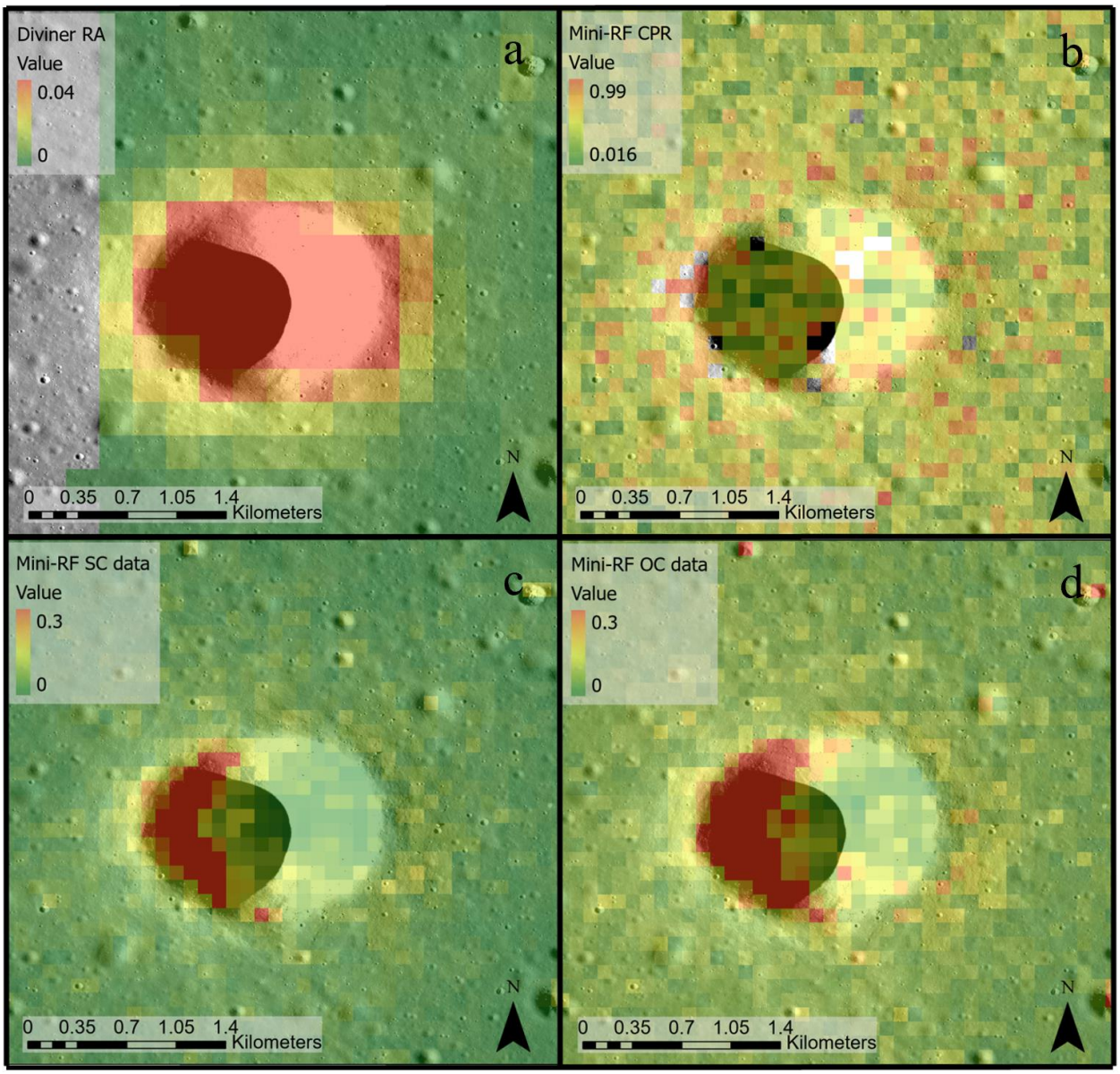

Figure 3. Diviner RA (a), Mini-RF CPR (b), SC (c), and OC data (d) overlaid onto crater an LROC NAC image of crater 8683 from the FT2014 crater database. This crater is located at 36.86° N, -15.9° E with a diameter of ~1.37 km and a modelled age of ~0.02 Ga.

4 Results

Our zonal statistics characterization algorithm includes mean, median, and percentile values of CPR and RA data for all impact craters in our dataset. A direct comparison of all individual impact craters in these datasets is unlikely to reveal clear trends due to noise in the Mini-RF CPR and Diviner RA datasets as well as the error that is inherent in the FT2014 diffusion model ages. This uncertainty, specifically the noise inherent in CPR measurements, has been documented in prior work (Ghent et al., 2016; Fassett et al., 2018; Nypaver et al., 2019). Therefore, we advise caution in using these methods of correlating remote sensing data and age as a means of establishing an independent age-dating method for individual craters. To mitigate this noise and provide a clearer understanding of the erosional processes occurring at lunar

impact craters, we bin the crater data values in 1000 κt increments and plot those bins as a function of increasing age.

For both crater rims and ejecta deposits, binned CPR and RA values generally trend to decrease over time (Fig. 4). Moreover, CPR and RA mean and median values associated with crater rims were elevated above ejecta deposit values for every crater bin over the lifetime of the lunar maria. To further characterize the observed trend, we used the York Method (York et al., 2004) to identify the least-squares fit line accounting for uncertainty in both CPR and RA. The slopes of the mean RA data for crater rims and ejecta (Fig. 4d) are distinguishable from each other (Table 1). Moreover, the slopes of the crater rim means in both data sets are statistically separable from zero. A difference of means test for all CPR and RA data bins indicates a higher degree of difference between the RA ejecta and rim data bins <0.6 Ga. The crater rim values reach a steady-state increase over the ejecta at ~2.0 Ga in both datasets. The difference between crater rim and ejecta values at the beginning of a crater's lifetime is ~0.06 in RA and ~0.1 in CPR. This difference in crater rim and ejecta RA and CPR decreases by ~60% and ~30% over the lifetime of the lunar mare, respectively.

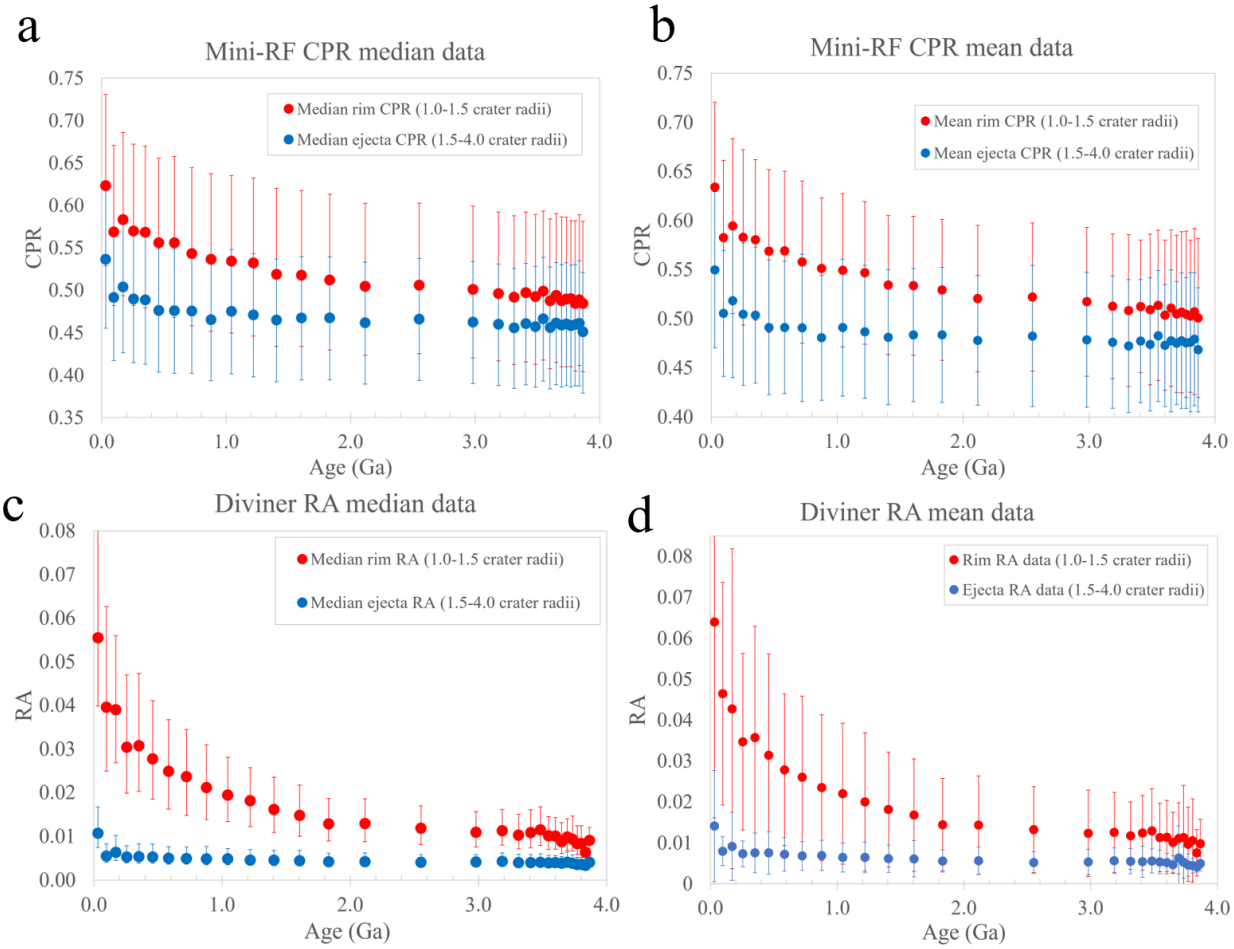

Figure 4. Binned CPR (a-b) and RA (c-d) median and mean values associated with the crater rim region (red points) and ejecta (blue points) shown as a function of increasing age. RA data associated with the crater rims is substantially decoupled from ejecta RA data (c-d) whereas the CPR signatures of crater rims and ejecta are within error of one another (a-b). In both datasets, the crater rims appear elevated above the ejecta for the lifetime of most craters in our dataset.

Error bars in Figs. 4a and 4c represent the 25th and 75th percentile data values of the respective bins whereas error bars in figs. 4b and 4d represent standard deviations.

	Ejecta data slope	Rim data slope
RA	-0.001+/-0.000	-0.006+/-0.002
CPR	-0.008+/-0.009	-0.022+/-0.011

Table 1. York fit slope values for the overall trends of binned CPR and RA mean values as a function of age (Figs. 3b and 3d.)

An analysis of Mini-RF SC radar albedo for the same crater bins from Fig. 5 reveals a similar trend to that of CPR and RA data with average SC albedo values decreasing over time (Fig. 5b). A similar relationship also exists in the evolution of SC albedo in that the impact crater rim SC values are elevated above the ejecta SC values for every bin in our dataset. A direct comparison of the crater rim and ejecta SC and OC radar albedo reveals separate trends both in slope and data distribution for those data bins (Fig. 5a). For Fig. 5a, we derived a linear fit using the York method and found that the rim data is best fit by a line of slope 1.03 ± 0.75, while the ejecta data is best fit by a line of slope 1.52 ± 1.78. Thus, while for the rim SC data provides information for the prediction of OC data and a positive linear correlation exists, within error ejecta SC values do not provide information for the prediction of ejecta OC values (i.e., the null hypothesis, that of a zero slope, cannot be ruled out). Our derived trend for crater rims is similar to that found by Virkki and Bhiravarasu (2019) for crater interiors and supports our interpretation of wavelength-scale scatterers on crater rims. The lack of a statistically robust trend for the ejecta SC and OC albedo values, along with their overall low albedo values compared to the rim, agrees with our interpretation of significant processing of wavelength-scale scatterers within the ejecta over time.

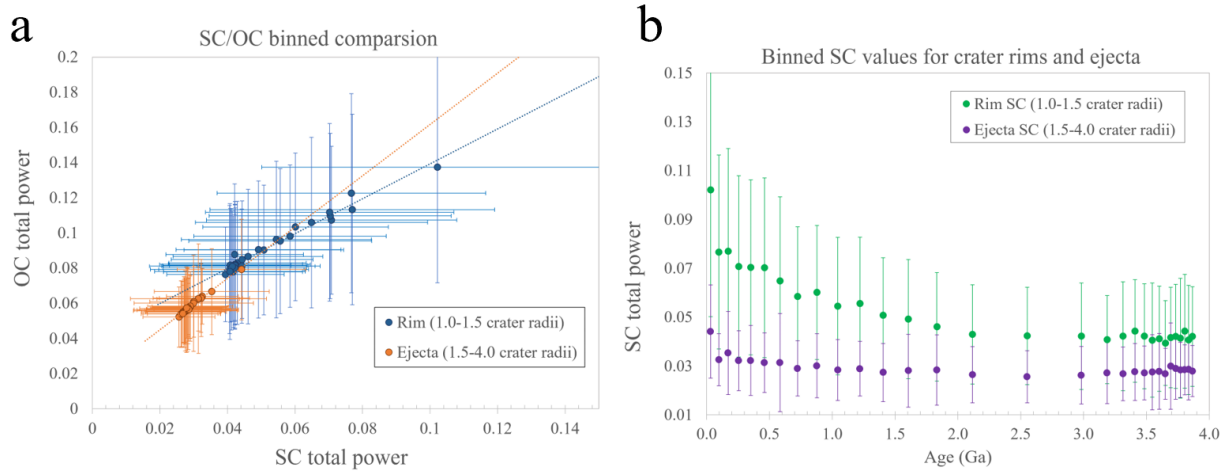

Figure 5. Binned SC (Same-sense radar albedo) for the same crater bins presented in Fig. 4 as a function of increasing age (a) and direct comparison of SC and OC radar albedo for those same bins. The SC data associated with the crater rims in (b) shows a similar trend to the RA and CPR data in Fig. 1 and is substantially decoupled from ejecta SC data. Based on the modelling results

of Virkki and Bhiravarasu (2019) the differences in slope and distribution of the ejecta and rim data in (a) appear to support our hypothesis of prolonged rim boulder presence.

5 Discussion

We interpret the data presented in Figs. 4–5 to indicate that boulders are present at the rims of impact craters on the lunar maria, not only during the early stages of an impact crater's existence on the lunar surface, but throughout the lifetimes of most craters in our dataset. Decreasing trends are observed for the RA and CPR data associated with impact crater rims and ejecta deposits as a function of time. Those trends indicate that surface and subsurface rocks at crater rims and ejecta deposits are breaking down over time. Decreasing differences between crater rim and ejecta data with time indicate that a steady state rock population may be reached at crater rims within ~2.0 Byr. That steady state rock population is then retained at crater rims for the duration of that crater's lifetime. The smaller difference between mean CPR ejecta and rim data slope relative to RA mean data is likely due to the sensitivity of the CPR data to subsurface rocks at the scale of the S-band wavelength. Though, this increased indifference in trend slope and the increased CPR standard deviation may also be attributable to the low signal-to-noise of the Mini-RF monostatic data. Without this sensitivity, the RA data show an increased disparity between crater rim and ejecta surface rock populations. The separation of impact crater rim and ejecta SC data is in agreement with the analysis of CPR and RA data and strongly supports the hypothesis that meter-scale boulders are present at impact crater rims for prolonged periods of time.

A direct comparison of crater rims and ejecta in Mini-RF SC and OC data (Fig. 5a) reveals distinct trends for these regions in both datasets. We base our interpretations of these trends on prior modelling of SC and OC scattering behaviors (Virkki and Bhiravarasu, 2019). Those authors utilized a discrete dipole approximation code to create a 4×4 covariance scattering matrix that approximates the effects of particle size, size distribution and refractive index on radar scattering. Their model held two of those variables constant while altering the third to show the effects of each. The results of those experiments indicate that an increase in wavelength scale scattering particles increases the backscattering enhancement factor and the overall length of the data distribution in a plot of SC and OC data. Furthermore, the slope of the data distribution best-fit line decreases with increasing backscattering enhancement factor. Based on that model, we infer that the increased distribution of binned crater rim data observed in our data is indicative of an increased number of wavelength-scale scatterers at crater rims. Moreover, the low SC and OC radar albedo values for the ejecta data is indicative of evolution towards a more porous regolith and increased cobble roundness in the ejecta with time (Fig. 5A). These interpretations are consistent with a higher degree of overturn in the regolith and boulder presence at crater rims.

Based on these results, we suggest that surface rock populations are maintained at simple crater rims by ongoing exhumation. This interpretation is not contradictory to earlier observed rates of boulder breakdown inferred from boulder counting methods. Rather, we suggest that mass wasting at crater rims occurs at a rate that exceeds the previously established rates of boulder breakdown. Mass wasting is, therefore, a dominant control on surface rock populations in that narrow annular zone. Prior work has shown that mass wasting processes are active on the lunar surface (e.g., Xie et al., 2017; Fassett and Thomson, 2014; Minton et al., 2019). It has also been shown that, over time, regolith from impact crater rims will incrementally fill crater

interiors, initially producing an increasing CPR signature in the crater interior for the first billion years, that then declines (Fassett et al., 2018b). Based on these prior studies and our findings in Figs. 4 and 5, we infer that subsurface rocks at impact crater rims are continually being uncovered as the overlying regolith migrates downslope into the crater interior of the crater ejecta. Some combination of past seismic activity and anomalous diffusion is the likely cause of the downslope motion of regolith from crater rims and is the same mechanism responsible for the topographic degradation of km-scale lunar craters and topography as a whole. At impact crater rims, anomalous diffusion and regolith transport must occur at a rate that exceeds the rate of regolith production, or at least the time it takes to break down exhumed rocks to scales smaller than detectable in the radar and RA datasets.

6 Conclusions

In this work we show that boulders are present at crater rims for prolonged periods of time, and we attribute their presence to rapid downslope transport of surface regolith. This conclusion is supported by both radar (CPR, SC, and OC) and thermal infrared (RA) remote sensing datasets. Qualitatively, large boulders are still observed at the rims of old, km-scale craters in LROC NAC images, and a visual crater rim/ejecta boulder dichotomy was reported by Schmitt et al., (2017) using Apollo 17 photographs (Fig. 6).

Figure 6. (Fig. 18 in Schmitt et al., 2017) Apollo 17 photograph taken by Astronaut Gene Cernan from the perspective of the rim of Camelot crater looking out into the associated ejecta deposit. A dichotomy is observed between the boulder population at the crater rim and in the ejecta deposit. NASA Photograph

In a re-analysis of Taurus Littrow valley geology, it was noted that there was a clear dichotomy between rock populations at the crater rim and in the ejecta deposit (Schmitt et al., 2017; Fig. 6). Those authors also cited a mechanism of continual regolith removal and rock exposure at the crater rim to explain their observations. It was also noted that the observed rocks at crater rims are likely to be in-situ, meaning that they underwent minimal transportation during the formation of the parent crater.

With the exception of several drill core samples from the Apollo and Luna programs, all lunar rock and soil samples were collected at the lunar surface where loose rocks were easily

attainable. As previous work has shown, rocks at the lunar surface are mostly comprised of ejecta material that has the capability to travel great distances from the parent crater during the crater formation process (e.g., Dundas and McEwen, 2007). Hence, one ongoing challenge in our understanding of lunar surface ages and composition lies in the assumption that our lunar samples were all relatively in situ at the time of collection. Attempts have been made to disentangle the source of lunar samples and mitigate the potential for distal source contamination, but if this assumption is incorrect and the samples that we have were transported from other areas of the Moon, some aspects of our understanding of lunar chronology and petrologic evolution may be flawed. The demonstration that rocks are exhumed over long periods of time at km-scale crater rims implies that those rocks being uncovered are locally derived. This finding provides a vital piece of information for future lunar sample return missions for which in-situ samples are desired for accurate chronological and petrological characterizations of the lunar surface units.

Acknowledgments and Data

We would like to acknowledge productive discussions with Nicholas Dygert, Molly McCanta, Catherine Neish, Sriram Bhiravarasu, Joshua Cahill, and members of the Mini-RF instrument science team that improved this effort. This work was supported in part by NASA LDAP NNX16AN57G to CIF and a grant from the Johns Hopkins University Applied Physics Laboratory through the NASA LRO mission. Data for all figures in this manuscript can be found at the following Figshare link: https://figshare.com/s/c90d69ba913757da5616 (This is currently a private link. The public DOI for these data will replace this link after publication of the manuscript).

References

Bandfield, J. L. et al. (2015), Lunar surface roughness derived from LRO Diviner radiometer observations. *Icarus*, 248, 357–372.

Bandfield, J. L. et al. (2011), Lunar surface rock abundance and regolith fines temperatures derived from LRO Diviner Radiometer data. *Journal of Geophysical Research*, 116, E00H02.

Bart, G., & H. Melosh (2010), Distributions of boulders ejected from lunar craters. *Icarus* (New York, N.Y. 1962), 209(2), 337–357. https://doi.org/10.1016/j.icarus.2010.05.023.

Basilevsky, A. T. et al. (2013), Survival times of meter-sized boulders on the surface of the Moon, *Planetary and Space Science*, 89, 118-126

Basilevsky, A. T. et al. (2015), Survival times of meter-sized rock boulders on the surface of airless bodies. *Planetary and Space Science*,117, 312–328.

Basilevsky, A. T. et al. (2018), Rock spatial densities on the rims and interiors of a group of Copernicus secondary craters. *Planetary and Space Science*,172, 14-21.

Cahill, J. S. et al. (2014), The miniature radio frequency instrument's (Mini-RF) global observations of Earth's Moon. *Icarus*, 243, 173–190.

Campbell, B. A. (2012), High circular polarization ratios in radar scattering from geologic targets. Journal of Geophysical Research, 11, E06008.

Campbell, M., & J. Ulrichs (1969), Electrical properties of rocks and their significance for lunar radar observations. *Journal of Geophysical Research*, 74(25), 5867–5881. https://doi.org/10.1029/JB074i025p05867

Craddock, R., & A. Howard (2000), Simulated degradation of lunar impact craters and a new method for age dating farside mare deposits. *Journal of Geophysical Research. Planets*.

Dundas, C. M., & A. S. McEwen (2007), Rays and secondary craters of Tycho. Icarus, 186, 31–40.

Fassett, C. et al. (2011), Thickness of proximal ejecta from the Orientale Basin from Lunar Orbiter Laser Altimeter (LOLA) data: Implications for multi-ring basin formation. *Geophysical Research Letters*, 38(17). https://doi.org/10.1029/2011GL048502

Fassett, C. I. & B. J. Thomson (2014), Crater degradation on the lunar maria: Topographic diffusion and the rate of erosion on the Moon. *Journal of Geophysical Research: Planets*, 119, 2255–227.

Fassett, C. I. et al. (2018a), Re-analysis of observations of crater degradation on the lunar maria accounting for anomalous diffusion. *Lunar Planet. Sci. Conf. 49th*, abstract 2083.

Fassett, C. I. et al. (2018b), Temporal evolution of S-band circular polarization ratios of kilometer-scale craters on the lunar maria. *Journal of Geophysical Research: Planets*, 123, 3133– 3143.

Gault, D. et al. (1972), Effects of microcratering on the lunar surface, *Geochem. Cosmochem A. cta, Suppt*, 3, 2713-2734.

Ghent, R. R. et al. (2014), Constraints on the recent rate of lunar ejecta breakdown and implications for crater ages. *Geology*, 42, pp. 1059-1062.

Ghent, R. R. et al. (2016), Lunar crater ejecta: physical properties revealed by radar and thermal infrared observations. *Icarus*, 273 pp. 182-195.

Haruyama, J., et al. (2012), Lunar global digital terrain model dataset produced from Selene (Kaguya) Terrain Camera stereo observations, *43rd Lunar Planet. Sci. Conf.*, 1200.

Horai, K. I. & G. Simmons (1972), Thermal property measurements on lunar material returned by Apollo 11 and 12 missions, Progress Astronaut. *Aeronaut*., 28, 243–267.

Hörz, F. et al. (1971), Micrometeorite craters on lunar rock surfaces. *Journal of Geophysical Research*, 76(23), 5770–5798. https://doi.org/10.1029/JB076i023p05770

Li, Y. et al. (2018), Correlations between ejecta boulder spatial density of small lunar craters and the crater age. *Planetary and Space Science*, 162, 52–61. https://doi.org/10.1016/j.pss.2017.08.007

Mazrouei, S., et al. (2019), Earth and Moon impact flux increased at the end of the Paleozoic. *Science*, 363(6424), 253–257.

Minton, D., et al. (2019), The equilibrium size-frequency distribution of small craters reveals the effects of distal ejecta on lunar landscape morphology. *Icarus* (New York, N.Y. 1962), 326, 63–87. https://doi.org/10.1016/j.icarus.2019.02.021

Molaro, J., & S. Byrne (2012), Rates of temperature change of airless landscapes and implications for thermal stress weathering. *Journal of Geophysical Research: Planets*, 117(E10). https://doi.org/10.1029/2012JE004138

Molaro, J. L. et al. (2017), Thermally induced stresses in boulders on airless body surfaces, and implications for rock breakdown. *Icarus*, 294, 247-261.

Neish, C., et al. (2013), A comparison of rayed craters on the Moon and Mercury. *Journal of Geophysical Research: Planets*, 118(10), 2247–2261. https://doi.org/10.1002/jgre.20166

Nypaver, C. N. (2019), Deriving lifetimes of lunar ejecta constituents: A model for lunar erosion and regolith overturn. Master's Thesis, University of Tennessee, 2019. https://trace.tennessee.edu/utk_gradthes/5500

Osinski, G., et al. (2011), Impact ejecta emplacement on terrestrial planets. *Earth and Planetary Science Letters*, 310(3-4), 167–181. https://doi.org/10.1016/j.epsl.2011.08.012

Raney, R. K. et al. (2011), The lunar Mini-RF radars: Hybrid polarimetric architecture and initial results, *Proc. IEEE*, 99(5), 808–823, doi:10.1109/JPROC.2010.2084970.

Robbins, S. J. et al. (2014), The variability of crater identification among expert and community crater analysts. *Icarus*, 234, 109–131. https://doi.org/10.1016/j.icarus.2014.02.02210.1029/2020JE006400

Ross, H. P. (1968), A simplified mathematical model for lunar crater erosion. *Journal of Geophysical Research*. 73, 1343–1354.

Schmidt, R., & K. Housen (1987), Some recent advances in the scaling of impact and explosion cratering. *International Journal of Impact Engineering*, 5(1), 543–560. https://doi.org/10.1016/0734-743X(87)90069-8

Schmitt, H., et al. (2017), Revisiting the field geology of Taurus–Littrow. *Icarus* (New York, N.Y. 1962), 298, 2–33. https://doi.org/10.1016/j.icarus.2016.11.042

Soderblom, L. A. (1970), A model for small-impact erosion applied to the lunar surface. *Journal of Geophysical Research.* 75, 2655–2661, doi:10.1029/JB075i014p02655.

Speyerer, E. et al., (2016), Quantifying crater production and regolith overturn on the Moon with temporal imaging. *Nature* (London), 538(7624), 215–218. https://doi.org/10.1038/nature19829

Stoffler, D. (2006), Cratering History and Lunar Chronology. *Reviews in Mineralogy and Geochemistry*, 60(1), 519–596. https://doi.org/10.2138/rmg.2006.60.05

Thompson, T. et al. (2011), Modeling radar scattering from icy lunar regoliths at 13 cm and 4 cm wavelengths. *Journal of Geophysical Research: Planets*, 116(E1). https://doi.org/10.1029/2009JE003368

Vickery, A. (1986). Size-velocity distribution of large ejecta fragments. *Icarus* 67 (2), 224–236.

Virkki, A. & Bhiravarasu, S. (2019), Modeling Radar Albedos of Laboratory-Characterized Particles: Application to the Lunar Surface. *Journal of Geophysical Research: Planets*, 124(11), 3025–3040. https://doi.org/10.1029/2019je006006

Wang, J. rt al., (2020), Quantitative Characterization of Impact Crater Materials on the Moon: Changes in Topographic Roughness and Thermophysical Properties with Age. *Journal of Geophysical Research: Planets*, 125(10). https://doi.org/10.1029/2019JE006091

Watkins, R., et al. (2019), Boulder Distributions Around Young, Small Lunar Impact Craters and Implications for Regolith Production Rates and Landing Site Safety. *Journal of Geophysical Research: Planets,* 124(11), 2754–2771. https://doi.org/10.1029/2019je005963

Xie, M. et al. (2017), Effect of Topography Degradation on Crater Size-Frequency Distributions: Implications for Populations of Small Craters and Age Dating: Effect of Topography Degradation on CSFD. *Geophysical Research Letters,* 44(20), 10–10,179. https://doi.org/10.1002/2017GL075298

York, D. et al. (2004), Unified equations for the slope, intercept, and standard errors of the best straight line. *American Journal of Physics,* 72(3), 367–375. https://doi.org/10.1119/1.1632486